

Communication

Growing Gold Nanostars on SiO₂ Nanoparticles: Easily Accessible, NIR Active Core–Shell Nanostructures from PVP/DMF Reduction

Laura C. Straub ¹, John A. Capobianco ² and Mathias S. Wickleder ^{1,*}

¹ Department of Chemistry, Institute of Inorganic Chemistry, University of Cologne, 50939 Cologne, Germany; laura.straub@uni-koeln.de

² Department of Chemistry and Biochemistry, Centre for NanoScience Research, Concordia University, Montreal QC H4B 1R6, Canada; john.capobianco@concordia.ca

* Correspondence: mathias.wickleder@uni-koeln.de

Abstract: A new synthesis strategy towards gold-coated silica nanoparticles is presented. The method provides an efficient, reliable and facile-coating process of well-defined star-shaped shell structures, characterized by UV-Vis, TEM, PXRD, DLS and zeta-potential measurements. A marked red shift of the Au-based plasmonic band to the region of the first biological window is observed offering great potential for future research of biological applications.

Keywords: core–shell nanostructures; gold nanostars; spiky shells



Citation: Straub, L.C.; Capobianco, J.A.; Wickleder, M.S. Growing Gold Nanostars on SiO₂ Nanoparticles: Easily Accessible, NIR Active Core–Shell Nanostructures from PVP/DMF Reduction. *Chemistry* **2022**, *4*, 647–654. <https://doi.org/10.3390/chemistry4030046>

Academic Editor: Ye Zhou

Received: 2 June 2022

Accepted: 16 June 2022

Published: 21 June 2022

Publisher's Note: MDPI stays neutral with regard to jurisdictional claims in published maps and institutional affiliations.



Copyright: © 2022 by the authors. Licensee MDPI, Basel, Switzerland. This article is an open access article distributed under the terms and conditions of the Creative Commons Attribution (CC BY) license (<https://creativecommons.org/licenses/by/4.0/>).

1. Introduction

Core–shell nanostructures attracted increasing attention in the late 1980s and early 1990s with the principle objectives to enhance the stability of nanoparticles, to functionalize the particles for disease targeting and employ their optical properties, for example in bioimaging and drug delivery [1–4]. A flurry of research activities in the following decades led to numerous nanoconstructs with potential applications in nanobiomedicine [5–9].

In the field of nanocomposites with dielectric cores covered by a metallic shell, gold-coated silica nanoparticles (SiO₂@Au) have garnered considerable attention. In 1998, Oldenburg et al., reported a colloid reduction process to synthesize gold nanoshells with different core and shell diameters with extinction wavelengths in the near-infrared (NIR) region. The synthesis is based on a stepwise growth of gold nanoparticles (AuNP) attached to the surface of silica nanoparticles (SiO₂-NP) [10]. Subsequently, substantial research has been carried out to obtain easily accessible gold coatings [11–14]. Presently, the scientific community continues work on overcoming the challenges of the long aging time required for the shell formation, to ameliorate the choice of reducing agents and to realize more efficient synthetic pathways.

Anisotropic gold nanostructures and SiO₂@Au exhibit similar extinction properties in the NIR [15]. For example, gold nanostars (AuNS) show unique surface plasmonic resonances (SPR) compared to spherical gold NP of the same size, caused by the formation of sharp edges. The red-shifted SPR band allows interaction with NIR light, which has higher tissue penetration as well as a good overlap with the first biological window within the region 600 to 1000 nm. The absorption of tissue components, such as melanin, oxy- and deoxyhemoglobin, reach a local minimum in this region which makes it attractive for biological applications [16]. From this perspective, both AuNS and SiO₂@Au are of particular interest for multiple biological applications and surface-enhanced spectroscopy [17–22]. Several synthetic routes for AuNS are known using spherical AuNP seeds [22–24]. The Liz-Marzán group synthesized high-yield AuNS using the reduction properties of *N,N*-dimethylformamide (DMF) combined with poly(vinylpyrrolidone) (PVP)

to prepare PVP-stabilized AuNS as well as AuNS containing a magnetite core [25,26]. In addition to PVP and DMF, other capping and reducing agents were used to synthesize spiky shells around polymer, magnetite as well as SiO₂-coated magnetite nanoparticles [27–30]. Combining the advantages of nanoshells and star-shaped structures, our research led to the investigation of star-shaped gold-coated silica nanoparticles (SiO₂@AuNS) shown in Figure 1.

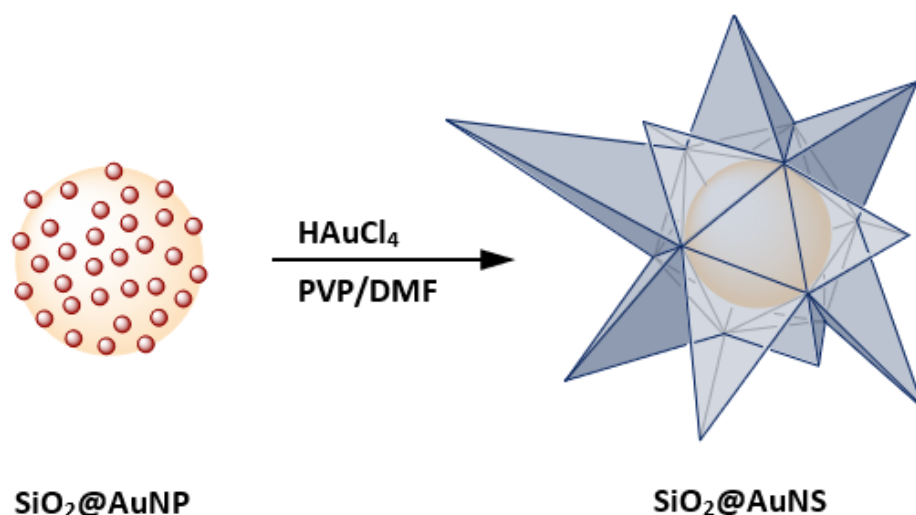


Figure 1. A schematic illustration of the SiO₂@AuNS core–shell formation based on the coating of SiO₂@AuNP in PVP/DMF in the presence of HAuCl₄.

Herein, we report the synthesis of a well-defined and size controllable nanostructure, SiO₂@AuNS, using SiO₂-NP cores. The developed synthetic procedure shows a major advantage over previously reported so-called spiky nanoshells because an easy coating approach for various silica-coated nanomaterials becomes accessible [27–29].

2. Materials and Methods

All chemicals were used as received without further purification. All glassware were cleaned with aqua regia and rinsed several times with water prior to use (Caution: strong oxidizer). UV-Vis data were recorded with a UV-1600PC (VWR, Radnor, PA, USA) in a quartz cuvette. DLS and zeta-potential measurements were performed with a Zetasizer (Malvern Panalytical, Malvern, UK) in PMMA cuvettes and folded capillary cells. The nanoparticles were dispersed in ethanol for DLS measurements and in water (pH 6.5) for zeta-potential measurements. TEM micrographs were recorded by using a LEO912 (ZEISS, Oberkochen, Germany) microscope operated at an acceleration voltage of 120 kV. A carbon film supported by a standard copper grid was used as sample carrier for TEM characterization. PXRD data were collected in sealed glass capillaries ($d = 0.9$ mm) with a Stadi-P (Stoe, Darmstadt, Germany) running with Mo-K α radiation and a Mythen detector in Debye–Scherrer geometry.

2.1. Synthesis of SiO₂-NH₂

Monodisperse core SiO₂-NP were prepared by a modified Stöber method [31]. The SiO₂-NP possess –OH on their surface which can be used for further surface modification. Thus, the SiO₂-NP were amine-functionalized using (3-aminopropyl)triethoxysilane (APTES). The amination was carried out by dispersing 500 mg of dry SiO₂-NP in 60 mL ethanol under sonication. In total, 3 mL of APTES was added dropwise and stirred overnight at room temperature. The amine-functionalized silica nanoparticles (SiO₂-NH₂) were isolated via centrifugation (8700 rpm, 10 min), washed three times with ethanol and dried at 60 °C for 12 h.

2.2. Synthesis of SiO₂@AuNP

Small, around 4 nm, citrate-stabilized AuNP were obtained by reducing chloroauric acid, (H₃O)AuCl₄·2H₂O, abbreviated as “HAuCl₄”, with sodium borohydride (NaBH₄) in the presence of sodium citrate [32]. Exchanging the citrate ligands with amine groups, the AuNPs were immobilized on the SiO₂-NP surface to form SiO₂@AuNP seed particles. Therefore, 25 mg of SiO₂-NH₂ was dispersed in water, 15 mL of the AuNP solution was slowly added and the mixture was allowed to react at room temperature. After centrifugation (8700 rpm, 15 min), an excess of unreacted AuNP was removed and the SiO₂@AuNP were washed three times with water. Redispersed in H₂O (5 mg/mL), the particles act as seeds for the core–shell synthesis.

2.3. Synthesis of SiO₂@AuNS

The star-shaped growth was obtained by adding various amounts (2.5, 5.0, 75.0, 1000 μL) of a solution of SiO₂@AuNP seeds to a solution containing 10 mM PVP (MW = 24,000) in DMF and 82 μL of 50 mM HAuCl₄ in aqueous media. The core–shell particles were stirred for 1 h and collected by centrifugation (8700 rpm, 15 min). The SiO₂@AuNS were washed three times with ethanol to remove an excess of PVP and redispersed in ethanol (7 mL).

3. Results and Discussion

The functionalized nanoparticles were characterized with suitable analytical methods using transmission electron microscopy (TEM), dynamic light scattering (DLS), zeta-potential measurements, UV-Vis measurements and powder X-ray diffraction (PXRD). The presence of the primary amine was confirmed via the use of the Ninhydrin test. TEM was performed to obtain the particle size distribution and revealed that the mean particle size of the prepared SiO₂-NH₂ nanoparticles to be 81.8 ± 7.6 nm. The zeta-potential is a measure of the magnitude of electrical repulsive forces between particles and is predictive of colloidal stability. Particles with zeta-potential greater than +25 mV or less than −25 mV typically have high degree of stability. This is described by the classical Derjaguin, Landau, Verwey, Overbeek (DLVO) theory of colloidal interaction, which predicts that in the absence of van der Waals attraction, the interaction between like-charged colloidal particles is repulsive [33,34]. The value of measured zeta-potential for the SiO₂-NH₂ nanoparticles is +19.8 mV which indicates a stable colloidal system that is absence of coagulation. In order to investigate the influence of sulfur with higher binding affinity to the AuNP, we used (3-mercaptopropyl)triethoxysilane (MPTS) to functionalize the SiO₂-NP and attach AuNP in the second step. No significant change was observed and the typical AuNP coverage of 30% that is reported in literature was not exceeded [35]. The successful synthesis of SiO₂@AuNP was verified by TEM and PXRD. Amorphous SiO₂-NP show only one broad diffuse peak at a value of 2θ of 10.7°, whereas for SiO₂@AuNP, five additional peaks appeared at 2θ of 17.3°, 19.7°, 28.5°, 33.6° and 35.1° which correspond to the reflections of the (111), (200), (220), (311) and (222) crystal planes of Au (see ESI Figure S1). The values are in good agreement with the theoretical pattern calculated from single-crystal data for the face-centered cubic structure of metallic Au with the space group *Fm-3m*.

For the star-shaped nanoshells, a color change from red to purple, blue or green was observed as a function of the concentration of the seeds (see Figure 2).

The resulting SiO₂@AuNS showed much stronger plasmonic resonance compared to the SiO₂@AuNP or AuNP and were synthesized in high yields (see ESI Figure S2). The nanostructures exhibit high stability over several months. The extinction spectra show slight red-shifts of the maxima associated with narrower bands (see ESI Figure S3).

Coating of the SiO₂@AuNP requires a sufficient amount of HAuCl₄ which is dependent on the surface area of the core SiO₂-NP. By adjusting the [HAuCl₄]/[seed] mass ratio (*R*), we were able to tune SiO₂@AuNS growth and the resulting properties. Table 1 summarizes the extinction maximum (λ_{max}), the diameter (d_{Au} and d_{hyrd}) of the growing gold nanostructures and the zeta-potentials (ζ) for different *R* values.

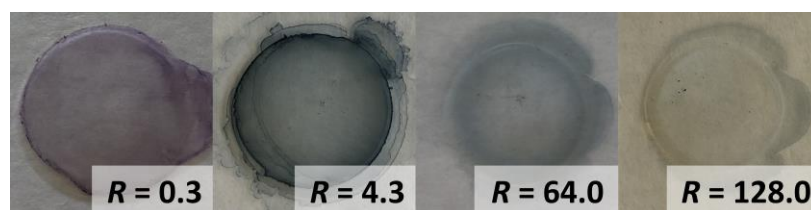


Figure 2. Colors of the synthesized gold nanostructures $\text{SiO}_2\text{@AuNS}$ immobilized on a glass substrate depending on the initial seed concentration. The color change indicated a red-shift of the plasmon band with increasing R .

Table 1. Overview of $[\text{HAuCl}_4]/[\text{seed}]$ ratio (R), extinction maxima (λ_{max}), the size of the gold nanostructure (d_{Au}) as well as the hydrodynamic diameter (d_{hydr}) and the zeta-potential (ζ) of the $\text{SiO}_2\text{-NH}_2$ nanoparticles or rather $\text{SiO}_2\text{@AuNP}$ before shell formation and coated $\text{SiO}_2\text{@AuNS}$ with varied amounts (1000–2.5 μL) of $\text{SiO}_2\text{@AuNP}$ seed solution.

	R	λ_{max} (nm)	d_{Au} (nm) ¹	d_{hydr} (nm) ²	ζ (mV)
$\text{SiO}_2\text{-NH}_2$	-	-	-	-	$+19.8 \pm 0.1$
$\text{SiO}_2\text{@AuNP}$	-	515.0	3.9 ± 1.2	- ⁴	-18.0 ± 0.9
$\text{SiO}_2\text{@AuNS}$	0.3	567.0	7.1 ± 0.9	- ⁴	-9.1 ± 2.0
	4.3	730.5	26.1 ± 6.7	- ⁴	-24.1 ± 1.7
	64.0 ³	814.0	107.8 ± 12.8	112.4 ± 1.1	-28.2 ± 1.1
	128.0	879.5	146.4 ± 17.2	147.3 ± 2.7	-29.4 ± 0.8

¹ Characterized by TEM measurements. ² Characterized by DLS measurements. ³ Critical ration (R_{min}). ⁴ No spiky shell formed.

The zeta-potentials presented in Table 1 show decreasing surface loadings depending on the stadium of the shell formation. While $\text{SiO}_2\text{-NH}_2$ show a positive zeta-potential caused by free amine groups, negative values were determined for the gold-decorated nanostructures. At higher R , i.e., higher gold loadings, lower zeta-potentials were observed. The amount of free amine functionalities decreases when they are linked to the gold surface during the immobilization of gold nanostructures. The more gold is bound to the $\text{SiO}_2\text{-NH}_2$ functions, the less free amine groups are detected, resulting in a negative zeta-potential.

The shell growth can not only be tracked by zeta potential measurements. Figure 3a shows the extinction spectra of the immobilized $\text{SiO}_2\text{@AuNP}$ seeds (dashed line) and the resulting $\text{SiO}_2\text{@AuNS}$ nanostructures (solid lines) depending on different R .

Corresponding TEM images of the nanostructures are presented in Figure 3b in order to monitor the actual shape of the formed nanostructure. By increasing R , the SPR bands exhibit a red-shift due to the growth of the gold nanostructure. Strong bathochromic shifts indicate the formation of sharp edges, which is well established for AuNS [24]. These growing steps of the gold nanostructures could be observed by TEM micrographs. High seed concentrations ($R = 0.3, 4.3$) only promoted the growth of AuNP but not the formation of a continuous crystalline metallic shell surrounding the $\text{SiO}_2\text{-NP}$. Above a critical $[\text{HAuCl}_4]/[\text{seed}]$ mass ratio (R_{min}) at circa 64.0, a core-shell structure was formed. Further variation in R leads to different sized $\text{SiO}_2\text{@AuNS}$. Therefore, the average nanostructure diameters were determined from the TEM images. At a high $\text{SiO}_2\text{@AuNP}$ seed concentration, equaling low R , the AuNP diameter d_{Au} increased from 3.9 nm initial seed diameter to 7.1 nm. The extinction spectra (Figure 3a, red line) show an equally shaped, slightly red-shifted SPR band compared to the initial seeds indicating the growth of gold nanospheres. For lower $\text{SiO}_2\text{@AuNP}$ concentrations, equaling higher R , an anisotropic growth occurs. When R is increased to a value of 4.3, branched nanostructures of 26.1 nm in diameter (green line) were formed. Extinction spectra and TEM images of three more nanostructures with R of 0.6, 3.2 and 12.8 line up perfectly in the trend shown here (see ESI Figures S4-1–S4-3). For R of 0.6 and 3.2, AuNP growth up to 20.4 nm is observed, with the subsequent change in the morphology of the nanoparticles (loss of spherical shape). Star-shaped particles were observed at a $R = 12.8$ ($d_{\text{Au}} = 46.0$ nm) with an extinction band

center at 766.0 nm. The nanostructures start to cover the SiO₂-NP, but a non-uniform shell was formed. A stronger bathochromic shift is observed due to the SPR resonance of the formed sharp edges. By exceeding R_{\min} , the star-shaped shells are formed (blue lines) and cause a strong red-shift of the SPR bands up to 879.5 nm indicating the formation of highly branched core-shell structures. Therefore, the SPR of the SiO₂@AuNS is found to be in the NIR region, similar to those of gold nanorods (AuNR) and SiO₂@Au shells [14,36]. The size of the SiO₂@AuNS is tuned by varying the ratio R . For $R = 64.0$, SiO₂@AuNS with a diameter of 108 nm were generated with a core diameter of 84 nm. Doubling the ratio produces SiO₂@AuNS with a diameter of 146 nm with a core diameter of 112 nm (see ESI Figures S5-1 and S5-2). DLS measurements confirmed the size distribution of the formed SiO₂@AuNS (see ESI Figure S6). With 112.4 nm and 147.2 nm, the hydrodynamic diameters are in good agreement with the diameters determined by TEM (see Table 1). Compared to the initial 81.8 nm SiO₂ cores, the smaller SiO₂@AuNS ($R = 64.0$) are coated with a gold shell of around 13 nm while a shell thickness of 32 nm was obtained for $R = 128.0$ including the tips of the spiky shell. Furthermore, broader extinction bands are observed for the core-shell nanostructures compared to the decorated cores. This observation can be traced back to the interaction of the spikes when a continuous shell is formed [37]. However, the SiO₂@AuNS show defined SPR centers in the desired NIR region and a significant trend correlated to the growing of the metallic nanostructures.

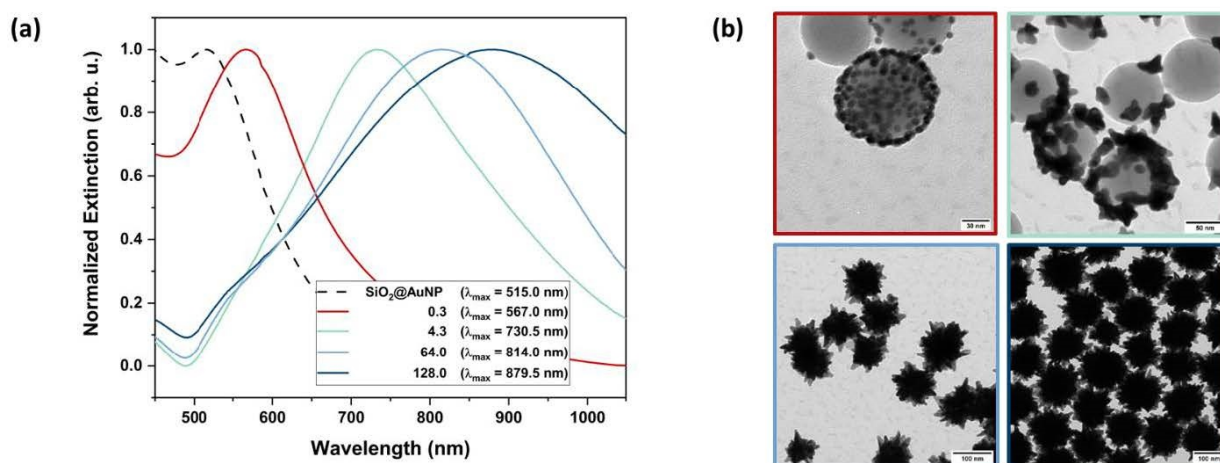


Figure 3. Characteristics of the formed nanostructures via UV-Vis and TEM. Extinction spectra (a) of the immobilized AuNP seeds (dashed line) and the resulting SiO₂@AuNS nanostructures after reaction with different [HAuCl₄]/[seed] mass ratios (solid lines). The according TEM images (b) show the stepwise growth of the gold nanostructure on the SiO₂-NP surface and are color-coded with respect to the UV-Vis spectra. The shell formation is observed for R larger than 64.

4. Conclusions

In conclusion, we have developed a reliable synthesis of easily accessible gold nanoshell formation on SiO₂ cores using the PVP/DMF reduction method. We succeeded in synthesizing SiO₂@AuNS core-shell nanoparticles of high stability with tunable shell thicknesses. The synthesis proceeded under mild conditions with short reaction times and simplifies the gold coating procedure significantly. This approach combines the advantages of SiO₂@Au and AuNS systems resulting in a perfect overlap of the SPR bands of the star-shaped gold nanostructures with the first biological window, providing a promising platform for plasmonic-enhanced NIR excitation for biological applications, e.g., in combination with upconversion nanoparticles. Beyond that, the coating approach is accessible for all SiO₂-coated nanostructures and therefore it is highly versatile as most of the nanomaterials can be coated with a SiO₂ shell.

Supplementary Materials: The following are available online at <https://www.mdpi.com/article/10.3390/chemistry4030046/s1>. Figure. S1 PXRD pattern of SiO₂(82nm) in black, SiO₂(82nm)@AuNP in red and the theoretical pattern for the face-centred cubic structure of metallic Au with the space group *Fm-3m*. Figure. S2 TEM image sections of SiO₂@AuNS(*R* = 128.0) demonstrating the high ratio of coated SiO₂ nanoparticles with 4,000 times magnification (a) and 10,000 times magnification (b). Figure. S3 TEM images of SiO₂@AuNS(*R* = 64.0, light blue) (a), and SiO₂@AuNS(*R* = 128.0, dark blue) (b) stored for seven month in ethanol and corresponding extinction spectra of the nanostructures (c). Solid lines show the initial spectra while dashed lines mark the spectra of the nanostructures recorded after seven month. Figure. S4–1 Extinction spectrum and TEM image of the SiO₂@AuNS for *R* = 0.6 (500.0 µL of the seed solution) with a gold nanostructure size of 11.3 ± 1.9 nm. Figure. S4–2 Extinction spectrum and TEM image of the SiO₂@AuNS for *R* = 3.2 (100.0 µL of the seed solution) with a gold nanostructure size of 20.4 ± 4.6 nm. Extinction spectrum and TEM image of the SiO₂@AuNS for *R* = 12.8 (25.0 µL of the seed solution) with a gold nanostructure size of 46.0 ± 12.8 nm. Figure. S4–3 Extinction spectrum and TEM image of the SiO₂@AuNS for *R* = 12.8 (25.0 µL of the seed solution) with a gold nanostructure size of 46.0 ± 12.8 nm. Figure. S5–1 Histograms of the core and the total diameter of SiO₂@AuNS (C) with a mass ratio of 64.0 (5.0 µL of the seed solution) determined by TEM. Figure. S5–2 Histograms of the core and the total diameter of SiO₂@AuNS (D) with a mass ratio of 128.0 (2.5 µL of the seed solution determined by TEM). Figure. S6 Normalized number-averaged DLS profiles of SiO₂@AuNS (*R* = 64.0) and SiO₂@AuNS (*R* = 128.0) dispersed in ethanol.

Author Contributions: L.C.S. synthesized and characterized the compounds and wrote the first draft; M.S.W. and J.A.C. reviewed and supervised the work. All authors have read and agreed to the published version of the manuscript.

Funding: This research received no external funding.

Institutional Review Board Statement: Not applicable.

Informed Consent Statement: Not applicable.

Data Availability Statement: Additional data can be found in the supporting informations. Primary data are available from the authors upon request.

Acknowledgments: L.C.S. gratefully acknowledges the support from the German Academic Exchange Service (DAAD) and MITACS. J.A.C. is a Concordia University Research Chair in Nanoscience and is grateful to Concordia University for financial support. J.A.C. is grateful to the Natural Science and Engineering Research Council (NSERC) of Canada for the sustained support of his research. We thank Silke Kremer for recording the powder diffraction data and Tabea von Keitz for technical assistance.

Conflicts of Interest: The authors declare no conflict of interest.

References

1. Youn, H.C.; Baral, S.; Fendler, J.H. Dihexadecyl phosphate, vesicle-stabilized and in situ generated mixed cadmium sulfide and zinc sulfide semiconductor particles: Preparation and utilization for photosensitized charge separation and hydrogen generation. *J. Phys. Chem.* **1988**, *92*, 6320–6327. [[CrossRef](#)]
2. Honma, I.; Sano, T.; Komiyama, H. Surface-Enhanced Raman Scattering (SERS) for Semiconductor Microcrystallites Observed in Ag-CdS Hybrid Particles. *J. Phys. Chem.* **1993**, *97*, 6692–6695. [[CrossRef](#)]
3. Zhou, H.S.; Sasahara, H.; Honma, I.; Komiyama, H.; Haus, J.W. Coated Semiconductor Nanoparticles: The CdS/PbS System's Photoluminescence Properties. *Chem. Mater.* **1994**, *6*, 1534–1541. [[CrossRef](#)]
4. Liz-Marzán, L.M.; Philipse, A.P. Synthesis and Optical Properties of Gold-Labeled Silica Particles. *J. Colloid Interface Sci.* **1995**, *176*, 459–466. [[CrossRef](#)]
5. He, L.; Dragavon, J.; Cho, S.; Mao, C.; Yildirim, A.; Ma, K.; Chattaraj, R.; Goodwin, A.P.; Park, W.; Cha, J.N. Self-assembled gold nanostar–NaYF₄:Yb/Er clusters for multimodal imaging, photothermal and photodynamic therapy. *J. Mater. Chem. B* **2016**, *4*, 4455–4461. [[CrossRef](#)]
6. Rojas-Gutierrez, P.A.; DeWolf, C.; Capobianco, J.A. Upconversion Nanoparticles: Formation of a Supported Lipid Bilayer on Faceted LiYF₄:Tm³⁺/Yb³⁺ Upconversion Nanoparticles (Part. Part. Syst. Charact. 12/2016). *Part. Part. Syst. Charact.* **2016**, *33*, 859. [[CrossRef](#)]
7. Zhao, L.; Ge, X.; Zhao, H.; Shi, L.; Capobianco, J.A.; Jin, D.; Sun, L. Double-Sensitive Drug Release System Based on MnO₂ Assembled Upconversion Nanoconstruct for Double-Model Guided Chemotherapy. *ACS Appl. Nano Mater.* **2018**, *1*, 1648–1656. [[CrossRef](#)]

8. Yousefi, S.R.; Alshamsi, H.A.; Amiri, O.; Salavati-Niasari, M. Synthesis, characterization and application of Co/Co₃O₄ nanocomposites as an effective photocatalyst for discoloration of organic dye contaminants in wastewater and antibacterial properties. *J. Mol. Liq.* **2021**, *337*, 116405. [[CrossRef](#)]
9. Mahdi, M.A.; Yousefi, S.R.; Jasim, L.S.; Salavati-Niasari, M. Green synthesis of DyBa₂Fe₃O_{7.988}/DyFeO₃ nanocomposites using almond extract with dual eco-friendly applications: Photocatalytic and antibacterial activities. *Int. J. Hydrogen Energy* **2022**, *47*, 14319–14330. [[CrossRef](#)]
10. Oldenburg, S.J.; Averitt, R.D.; Westcott, S.L.; Halas, N.J. Nanoengineering of optical resonances. *Chem. Phys. Lett.* **1998**, *288*, 243–247. [[CrossRef](#)]
11. Brinson, B.E.; Lassiter, J.B.; Levin, C.S.; Bardhan, R.; Mirin, N.; Halas, N.J. Nanoshells Made Easy: Improving Au Layer Growth on Nanoparticle Surfaces. *Langmuir* **2008**, *24*, 14166–14171. [[CrossRef](#)] [[PubMed](#)]
12. Ignacio-De Leon, P.A.A.; Zharov, I. SiO₂@Au Core–Shell Nanospheres Self-Assemble To Form Colloidal Crystals That Can Be Sintered and Surface Modified To Produce pH-Controlled Membranes. *Langmuir* **2013**, *29*, 3749–3756. [[CrossRef](#)] [[PubMed](#)]
13. Schlather, A.E.; Manjavacas, A.; Lauchner, A.; Marangoni, V.S.; DeSantis, C.J.; Nordlander, P.; Halas, N.J. Hot Hole Photoelectrochemistry on Au@SiO₂@Au Nanoparticles. *J. Phys. Chem. Lett.* **2017**, *8*, 2060–2067. [[CrossRef](#)]
14. Zhang, X.; Ye, S.; Zhang, X.; Wu, L. Optical properties of SiO₂@M (M = Au, Pd, Pt) core–shell nanoparticles: Material dependence and damping mechanisms. *J. Mater. Chem. C* **2015**, *3*, 2282–2290. [[CrossRef](#)]
15. Li, N.; Zhao, P.; Astruc, D. Anisotropic Gold Nanoparticles: Synthesis, Properties, Applications, and Toxicity. *Angew. Chem. Int. Ed.* **2014**, *53*, 1756–1789. [[CrossRef](#)]
16. Richards-Kortum, R.; Sevick-Muraca, E. Quantitative optical spectroscopy for tissue diagnosis. *Annu. Rev. Phys. Chem.* **1996**, *47*, 555–606. [[CrossRef](#)] [[PubMed](#)]
17. Hirsch, L.R.; Stafford, R.J.; Bankson, J.A.; Sershen, S.R.; Rivera, B.; Price, R.E.; Hazle, J.D.; Halas, N.J.; West, J.L. Nanoshell-mediated near-infrared thermal therapy of tumors under magnetic resonance guidance. *Proc. Natl. Acad. Sci. USA* **2003**, *100*, 13549–13554. [[CrossRef](#)]
18. Jain, P.K.; Lee, K.S.; El-Sayed, I.H.; El-Sayed, M.A. Calculated Absorption and Scattering Properties of Gold Nanoparticles of Different Size, Shape, and Composition: Applications in Biological Imaging and Biomedicine. *J. Phys. Chem. B* **2006**, *110*, 7238–7248. [[CrossRef](#)]
19. Fales, A.M.; Yuan, H.; Vo-Dinh, T. Silica-Coated Gold Nanostars for Combined Surface-Enhanced Raman Scattering (SERS) Detection and Singlet-Oxygen Generation: A Potential NanoplatforM for Theranostics. *Langmuir* **2011**, *27*, 12186–12190. [[CrossRef](#)]
20. Hernández-Montoto, A.; Gorbe, M.; Llopis-Lorente, A.; Terrés, J.M.; Montes, R.; Cao-Milán, R.; de Greñu, B.D.; Alfonso, M.; Orzaez, M.; Marcos, M.D.; et al. A NIR light-triggered drug delivery system using core–shell gold nanostars–mesoporous silica nanoparticles based on multiphoton absorption photo-dissociation of 2-nitrobenzyl PEG. *Chem. Commun.* **2019**, *55*, 9039–9042. [[CrossRef](#)]
21. Lal, S.; Grady, N.K.; Kundu, J.; Levin, C.S.; Lassiter, J.B.; Halas, N.J. Tailoring plasmonic substrates for surface enhanced spectroscopies. *Chem. Soc. Rev.* **2008**, *37*, 898–911. [[CrossRef](#)] [[PubMed](#)]
22. Quintanilla, M.; García, I.; de Lázaro, I.; García-Alvarez, R.; Henriksen-Lacey, M.; Vranic, S.; Kostarelos, K.; Liz-Marzán, L.M. Theranostics Thermal Monitoring during Photothermia: Hybrid Probes for Simultaneous Plasmonic Heating and near-Infrared Optical Nanothermometry. *Theranostics* **2019**, *9*, 7298–7312. [[CrossRef](#)] [[PubMed](#)]
23. Niu, W.; Chua, Y.A.A.; Zhang, W.; Huang, H.; Lu, X. Highly Symmetric Gold Nanostars: Crystallographic Control and Surface-Enhanced Raman Scattering Property. *J. Am. Chem. Soc.* **2015**, *137*, 10460–10463. [[CrossRef](#)] [[PubMed](#)]
24. Trigari, S.; Rindi, A.; Margheri, G.; Sottini, S.; Dellepiane, G.; Giorgetti, E. Synthesis and modelling of gold nanostars with tunable morphology and extinction spectrum. *J. Mater. Chem.* **2011**, *21*, 6531–6540. [[CrossRef](#)]
25. Kumar, P.S.; Pastoriza-Santos, I.; Rodriguez-Gonzalez, B.; De Abajo, F.J.G.; Liz-Marzán, L.M. High-yield synthesis and optical response of gold nanostars. *Nanotechnology* **2007**, *19*, 015606. [[CrossRef](#)]
26. Quaresma, P.; Osório, I.; Dória, G.; Carvalho, P.A.; Pereira, A.; Langer, J.; Araújo, J.P.; Pastoriza-Santos, I.; Liz-Marzán, L.M.; Franco, R.; et al. Star-shaped magnetite@gold nanoparticles for protein magnetic separation and SERS detection. *RSC Adv.* **2014**, *4*, 3659–3667. [[CrossRef](#)]
27. Sanchez-Gaytan, B.L.; Park, S.-J. Spiky Gold Nanoshells. *Langmuir* **2010**, *26*, 19170–19174. [[CrossRef](#)]
28. Wei, Q.; Song, H.-M.; Leonov, A.P.; Hale, J.A.; Oh, D.; Ong, Q.K.; Ritchie, K.; Wei, A. Gyromagnetic Imaging: Dynamic Optical Contrast Using Gold Nanostars with Magnetic Cores. *J. Am. Chem. Soc.* **2009**, *131*, 9728. [[CrossRef](#)]
29. Hu, Y.; Wang, R.; Wang, S.; Ding, L.; Li, J.; Luo, Y.; Wang, X.; Shen, M.; Shi, X. Multifunctional Fe₃O₄@Au core/shell nanostars: A unique platform for multimode imaging and photothermal therapy of tumors. *Sci. Rep.* **2016**, *6*, 28325. [[CrossRef](#)]
30. Bedford, E.E.; Boujday, S.; Pradier, C.-M.; Gu, F.X. Spiky gold shells on magnetic particles for DNA biosensors. *Talanta* **2018**, *182*, 259–266. [[CrossRef](#)]
31. Stöber, W.; Fink, A.; Bohn, E. Controlled growth of monodisperse silica spheres in the micron size range. *J. Colloid Interface Sci.* **1968**, *26*, 62–69. [[CrossRef](#)]
32. Lu, L.; Randjelovic, I.; Capek, R.; Gaponik, N.; Yang, J.; Zhang, H.; Eychmüller, A. Controlled Fabrication of Gold-Coated 3D Ordered Colloidal Crystal Films and Their Application in Surface-Enhanced Raman Spectroscopy. *Chem. Mater.* **2005**, *17*, 5731–5736. [[CrossRef](#)]

33. Derjaguin, B.; Landau, L.D. Theory of the Stability of Strongly Charged Lyophobic Sols and of the Adhesion of Strongly Charged Particles in Solutions of Electrolytes. *Acta Physicochim. URSS* **1941**, *14*, 633–662. [[CrossRef](#)]
34. Verwey, E.J.W.; Overbeek, J.T.h.G. Theory of the Stability of Lyophobic Colloids. In *The Interaction of Sol Particles Having an Electric Double Layer*; Elsevier Pub. Co.: Amsterdam, The Netherlands, 1962.
35. Wang, H.; Brandl, D.W.; Le, F.; Nordlander, P.; Halas, N. Nanorice: A Hybrid Plasmonic Nanostructure. *Nano Lett.* **2006**, *6*, 827–832. [[CrossRef](#)]
36. Murphy, C.J.; Sau, T.K.; Gole, A.M.; Orendorff, C.J.; Gao, J.; Gou, L.; Hunyadi, S.E.; Li, T. Anisotropic Metal Nanoparticles: Synthesis, Assembly, and Optical Applications. *J. Phys. Chem. B* **2005**, *109*, 13857–13870. [[CrossRef](#)] [[PubMed](#)]
37. Sanchez-Gaytan, B.L.; Qian, Z.; Hastings, S.P.; Reza, M.L.; Fakhraei, Z.; Park, S.-J. Controlling the Topography and Surface Plasmon Resonance of Gold Nanoshells by a Templated Surfactant-Assisted Seed Growth Method. *J. Phys. Chem. C* **2013**, *117*, 8916–8923. [[CrossRef](#)]